Supporting Information

Calebiro et al. 10.1073/pnas.1205798110

SI Results

Calibration with Single Fluorophores. To calibrate the method, the cell-impermeant Alexafluor 647 BG derivative (Alexa647-BG) was spotted on clean glass coverslips that were imaged by total internal reflection fluorescence microscopy (TIRF-M). At low densities, diffraction-limited particles were visible (Fig. S1*A*). Here and below, particles were automatically detected and tracked using recently described algorithms (1). These particles represented single molecules, as indicated by the fact that they bleached in one step (Fig. S1*B*). The corresponding particle intensity distribution is shown in Fig. S1*C*. A single peak of intensity 0.0192 ± 0.0050 (mean ± SD) was observed, further supporting the notion that these were single fluorophore molecules.

Validation with Simulated Particles. Simulated data, consisting of computer-generated image sequences of single particles with Brownian motion, were created (Fig. S4*A* and Movie S3) and analyzed as described for SNAP-CD86 image sequences. Particles were simulated with an intensity distribution, diffusion speed, and bleaching behavior similar to those of SNAP-CD86 particles. Random noise was added to the image sequences to obtain a signal-to-noise ratio comparable to that of SNAP-CD86 images. The analysis with the Gaussian fitting algorithm revealed the presence of a largely predominant peak corresponding to monomeric particles and a minor peak of approximately double intensity (Fig. S4 *B* and *C*), ascribable to the random colocalization of two particles at a distance below the resolution limit of the system. As predicted on the basis of the calculation of the probability that two particles are found in such close proximity, the fraction of particles that for this reason were erroneously identified as apparently dimeric was growing nonlinearly with increasing particle density (Fig. S4 *D* and *E*). These data provided an estimate of the accuracy and limits of the analysis. For densities below 0.45 particle/μm^2, the occurrence of apparent dimers was particularly low, ∼5–13%, and most particles were correctly identified as monomers. The small differences observed between simulations and experimental data here as well as elsewhere (2) could be due to a number of reasons. A possible explanation is that the plasma membrane is a highly crowded (about 30% of its surface is covered by proteins) and complex environment. Interestingly, previous studies have found that although cell-surface G-protein–coupled receptors (GPCRs) and other cell-surface molecules apparently diffuse randomly (at least when observed with the temporal resolutions commonly attainable and used in the present study), they undergo "hop diffusion" when observed at very high speed (in the microsecond range) (3). On the basis of this observation, these authors proposed a model in which the diffusion of plasma-membrane molecules occurs as "hop" movements between adjacent microcompartments of the size of ∼200–300 nm, delimited by the cortical cytoskeleton. The occurrence of such hop diffusion would not cause appreciable changes in the apparent diffusion of GPCR particles measured at our temporal resolution, but could alter the probability of "random colocalizations" between two particles. To verify this possibility, we have performed an additional series of simulations in which particles macroscopically diffuse with the same apparent diffusion coefficient as in previous simulations, but diffuse 10 times faster within 300-nm compartments in which they reside for 100 ms. Interestingly, these simulations were associated with colocalization rates (Fig S4 *D* and *E*, red data) that are almost identical to those obtained with SNAP-CD86. Thus, the apparent small discrepancy between simulated and SNAP-CD86 data can be solved by using a more complex model of particle behavior. Importantly, such deviations from pure random diffusion occur on a temporal (and spatial) scale, which is below that of our measurements and much lower than that involved in random colocalization or true interactions. Thus, these deviations do not significantly affect the lifetimes of colocalizations such as those reported in Fig. 3. These simulations also allowed us to verify the accuracy of our analysis at different receptor densities. Noteworthy, the percentage of apparent dimers as well as the accuracy of particle detection and tracking began to deteriorate above 0.45 particle/μm^2. For this reason, only movies with densities below this value were analyzed in all subsequent experiments.

Correction for Apparent Colocalizations. A mathematical model was developed to correct the results of the mixed Gaussian fitting analyses for the presence of random colocalizations. Results obtained with control monomeric receptors (SNAP-CD86) as well as with simulated monomeric particles showed that the density of apparent dimers was growing with the second power of receptor density (Fig. S8*A*). On the basis of this information, we developed a system of nonlinear equations that allowed us to estimate the underlying distribution of receptor particles without random colocalizations (details in *SI Materials and Methods*). This approach was able to efficiently correct the distributions obtained with control SNAP-CD86 and SNAP2×-CD86 receptors (Fig. S8*B*). Application of the same correction to results obtained with GPCR constructs was associated with limited changes in the corresponding distributions as shown by a representative example in which this correction was applied to data obtained with γ-amino butyric acid ($GABA_B$) receptors (Fig. S8*C*).

SI Materials and Methods

Plasmids. A plasmid coding for an N-terminally FLAG-tagged human β_2-adrenergic receptor (β_2AR) was previously described (4). A plasmid coding for FLAG-tagged human β_1-adrenergic receptor (β_1AR) was cloned using the same strategy. SNAP-β_1AR and SNAP-β_2AR were generated by inserting the SNAP-tag directly after the FLAG sequence in the previous constructs. These constructs were functional, as shown by normal radioligand binding and cAMP concentration-response dependencies (Fig. S5). Plasmids SNAP-CD86 and SNAP2×-CD86 were generated by replacing YFP with either one or two copies of SNAP in a previously described construct coding for CD86 with YFP fused at its N terminus (5). Plasmids coding for wild-type human $GABA_{B1a}$ and $GABA_{B2}$ receptors as well as human $GABA_{B1a}$ and $GABA_{B2}$ with the SNAP-tag fused at their N termini (SNAP-$GABA_{B1}$ and SNAP-$GABA_{B2}$) were kindly provided by J. P. Pin (Institut de Génomique Fonctionnelle, Université Montpellier, Montpellier, France) and were shown to be functional in a previous study (6).

Coverslip Cleaning. Twenty-four-millimeter glass coverslips were extensively cleaned to remove any background fluorescence. First, they were sonicated in a solution containing 5 M NaOH for 1 h. After three washes with distilled water, they were dried and further sonicated in chloroform for 1 h. Coverslips were then dried and stored in 100% ethanol until use.

Generation of Stable HEK293 Cell Line. HEK293 cells were cultured in DMEM, supplemented with 10% (vol/vol) FCS, penicillin, and streptomycin at 37 °C and in the presence of 5% (vol/vol) CO_2. For the generation of the stable cell line expressing SNAP-β_1AR,

HEK293 cells were transfected with Effectene (Qiagen), following the manufacturer's protocol. After selection with 1.3 mg/mL G418, individual clones were obtained by limiting dilution and the clone with best cell-surface SNAP-β_1AR expression was used.

Determination of Alexa647-BG Labeling Efficiency. HEK293 cells stably expressing β_1AR were plated at a density of 100,000 cells per well in 96-well imaging plates (BD Biosciences) precoated with poly-D-lysine. Cells were labeled with different concentrations of Alexa647-BG in complete medium for 30 min at 37 °C and washed twice with complete medium. Thereafter, they were stained with 1 μg/mL Hoechst 33345 for 30 min at 37 °C and washed three times with PBS. Fluorescent images of Alexa647-BG and Hoechst 33345 were acquired with an automated imaging system (Pathway; BD Biosciences).

Radioligand Binding. Radioligand binding experiments were performed as previously described (7). Briefly, CHO cells were plated in 20-cm Petri dishes at a density of 1.3×10^7 and transfected with 60 μg plasmid DNA + 180 μL lipofectamine 2000. Cells were homogenized 48 h after transfection and membranes of transfected and mock-transfected CHO cells were incubated with 50 pM [^{125}I]iodocyanopindolol (^{125}I-CYP; Amersham Biosciences) and the indicated concentrations of bisprolol or ICI-118551 for 90 min at room temperature, filtered through Whatman GF/F filters, and washed three times with ice-cold assay buffer. Samples were counted in a γ-counter (Wallac 1480 wizard 3″).

Measurement of cAMP Concentrations. cAMP measurements were performed by a RIA, using standard procedures. Briefly, cells were preincubated in Krebs–Ringer–Hepes buffer containing 300 μM 3-isobutyl-1-methylxanthine (IBMX) for 30 min at 37 °C. Thereafter, they were stimulated with different concentrations of isoproterenol in the same buffer for 60 min at 37 °C. At the end of the incubation the medium was discarded and samples were extracted with 0.1 M HCl. The cell extracts were dried in a vacuum concentrator, resuspended in water, and diluted. cAMP concentrations were measured by a RIA according to the method of Brooker et al. (8).

Latrunculin A Treatment and Actin Staining. CHO cells were transfected and labeled with Alexa647-BG as described above. Subsequently, cells were incubated with 5 μM latrunculin A (Sigma-Aldrich) for 30 min at 37 °C. For F-actin staining, cells were then fixed with 4% (wt/vol) paraformaldehyde in PBS for 10 min, permeabilized with 0.1% Triton X100 for 3 min, and blocked with 3% (wt/vol) BSA for 20 min, all at room temperature. Cells were then incubated with 16 nM Alexafluor 488-phalloidin (Invitrogen) for 30 min at 37 °C.

Computational Analyses. Particles were detected and tracked using recently described algorithms (1) implemented in Matlab (The MathWorks). Briefly, the subpixel location and intensity above background of diffraction-limited particles are calculated by fitting a 2D Gaussian with the SD of the spread point function of the microscope around local intensity maxima. Tracking is performed on the basis of an approximation of the multiple-hypothesis tracking approach. Specifically, for each step and each particle a cost is assigned to every potential event (e.g., particle blinking, merging, splitting, appearing, or disappearing) and the solution that minimizes the sum of the costs is selected. This allows us also to track a particle beyond a blinking event, which is not possible with other tracking algorithms (details in ref. 1). The blinking frequency measured in our tracks by dividing the number of blinking events by the total duration of the tracks was low—approximately one event every 1,000 frames per fluorophore—and the duration of a blinking event was relatively short, typically 5–10 frames. The outcome of the tracking analysis contains the position and intensity of each particle at each frame as well as information about merging and splitting events. At the signal-to-noise ratio typical of our single-molecule images, two particles were recognized as merged once their distance fell below ∼300 nm (details in ref. 1). Particle intensities are expressed as the amplitude values of the Gaussian fit (1) (this Gaussian fitting used for particle detection should not be confounded with the subsequent mixed Gaussian fitting analysis that was implemented to assess particle di-/oligomerization). This approach allows to get intensities for two or more particles even when they are very close or partially overlapping, due to the fact that if a spot size is statistically bigger than expected on the basis of the measured point spread function (PSF), the detection software attempts to fit more kernels (i.e., partially overlapping Gaussians), the amplitudes of which can be used as estimates of the intensity of each underlying particle. The cell-surface area was measured by calculating the area of a binary mask that was manually drawn following the contour of the analyzed cell. The particle density was obtained by dividing the number of detected particles located within the binary mask at the beginning of the movie by the cell-surface area. The correctness of this calculation was verified by manual inspection. Most particles were detected until they bleached/disappeared or merged with other particles. The mean track duration was ∼4.5 s (min = 0.48 s; max = 57.6 s). The background was estimated on the basis of the values provided by the detection algorithm, which for the detection of local maxima calculates the local background by excluding outliers represented by the fluorescent particles and performing a moving average. Values are expressed as fractions of the maximal intensity value that can be assigned to a pixel. The background values were very similar for both real movies and simulations (about 0.03–0.04 for both). This was also true for the SD of the background (i.e., noise), which was about 0.002–0.004 for both real movies and simulations.

Data were visualized and further analyzed using additional Matlab algorithms that we developed for this purpose and that are described below.

Mixed Gaussian fitting. The distributions of particle intensities were analyzed by performing a mixed Gaussian fitting. For each particle, we averaged the intensity from the beginning of the movie to the frame before the first stepwise change in intensity (generally down, due to a photobleaching event) occurred, up to a maximum of 20 frames. Changes in intensity were detected by fitting the intensity data with a step fitting algorithm (below). As there are several sources of variability in the intensity of a single dye, data are dispersed and their distribution can be approximated to a normal distribution. For cells containing a mixture of monomers and oligomers, intensities are expected to have a distribution corresponding to the sum of Gaussians with different mean values. The mixed Gaussian model used for the fitting can be described by the equation

$$\varphi(i) = \sum_{n=1}^{n_{max}} A_n \cdot \frac{1}{\sigma\sqrt{2\pi}} e^{-\frac{(i-\mu\cdot n)^2}{2(\sigma\cdot n)^2}},$$

where $\varphi(i)$ is the frequency of particles having intensity i, n is the component number, and A_n is the area under the curve of component n. μ and σ are the mean and SD of reference single fluorophores. The maximal number of components (n_{max}) was determined for each image sequence by progressively increasing n_{max} until the addition of one component no longer resulted in a statistically better fitting, as judged by an F-test ($P > 0.05$). The denominator $2(\sigma\cdot n)^2$ was used because, likely as a consequence of the known local inhomogeneities of the cell surface and TIRF illumination, the position of the particles was found to be the major source of variation in particle intensity. Thus, fluorophores located in the same spot were not considered independent (9).

The intensity distribution of monomeric receptors (Alexa647-labeled SNAP-CD86) was used as an initial estimate of μ and σ. However, because there can be minor differences in particle intensities among different image sequences, μ- and σ-values were fine adjusted for each individual image sequence by performing a first mixed Gaussian fitting on the last 60 frames, when a large fraction of fluorophores was photobleached and a predominant peak corresponding to the intensity of single fluorophores should be present. Also in this case, intensity averaging was performed on data only before a change in intensity was detected by the step-fitting algorithm. The obtained μ- and σ-values were then used in a second mixed Gaussian fitting on the first 20 frames of image sequences to estimate the actual abundance of each particle component. The weight of each individual component was calculated from A_n values. Confidence limits for the intensity of a single fluorophore were on average ±5% (range: 1.6–11.4%). Concerning the fractions of the components, for fractions of amplitude >5 particles, the confidence limits were on average ±27% (range: 18–37%). For very small fractions (amplitude <5 particles), they were on average ±59% (range: 26–96%). R^2 values for the mixed Gaussian fitting analyses performed in this study were 0.87 ± 0.07 (mean ± SD).

Step fitting. A simple algorithm was developed to perform a step fitting of the intensity profile of each particle. For each iteration i, the algorithm assigns an increasing value to the step size s_i, within the interval $\mu \pm \sigma$, where μ and σ are the mean and standard values of the intensities of a single fluorophore, estimated for each image sequence as described above (*Mixed Gaussian fitting*). Intensities that fall within $\frac{1}{2}s_i n$ and $2s_i n$, where n is the number of molecules of intensity s_i, are assigned the value $s_i n$ in the fitted data. Very fast changes due to noise are excluded from the fitting. For each iteration, the residuals (r_i) between the observed and fitted data are calculated. This value is multiplied by two independent penalty factors to give a final score Z_i for each iteration, based on the formula

$$Z_i = r_i \cdot \left(1 + p_i^{ms} + p_i^{ss}\right),$$

where p_i^{ms} is a penalty for the presence of missing steps and p_i^{ss} is a penalty for choosing s_i far from μ. The solution that minimizes Z_i is finally selected.

The penalty p_i^{ms} was introduced to penalize solutions that contain missing steps and is calculated according to the formula

$$p_i^{ms} = \alpha^{ms} \cdot n_i^{ms},$$

where α^{ms} is an arbitrary constant and n_i^{ms} is the number of missing steps.

The penalty p_i^{ss} was introduced to penalize solutions that use s_i far from μ. Such a penalty is calculated on the basis of the intensity distribution of single fluorophores, according to the formula

$$p_i^{ss} = \alpha^{ss} \cdot \left(1 - e^{-\frac{(s_i-\mu)^2}{2\sigma^2}}\right),$$

where α^{ss} is an arbitrary constant.

Diffusion speed. The diffusion speed of receptor particles was calculated on the basis of their mean square displacement (MSD). For each particle and every time interval t, the MSD was calculated according to the formula

$$\mathrm{MSD}(t) = \mathrm{MSD}(n \cdot fr_{time}) = \frac{1}{N} \sum_{i=1}^{N} \left[(x_{i+n} - x_i)^2 + (y_{i+n} - y_i)^2\right],$$

where N is the number of steps analyzed, n is the step size in frames ranging from 1 to 1/10 of the available frames, fr_{time} is the time between two consecutive frames, and x and y describe the particle position at the frame indicated by the indexes. Diffusion coefficients (D) were then calculated by fitting data with the following equation:

$$\mathrm{MSD} = 4Dt.$$

Lifetime of interactions. The duration of each colocalization between two particles (Δt) was calculated on the basis of the merging and splitting information derived from the tracking analysis. Particles showing bleaching during the analysis time window were excluded. Using these data, the apparent lifetime of particle colocalizations (τ^*) was calculated by fitting data with the equation

$$I = I' \cdot e^{-\frac{t}{\tau^*}},$$

where I is the number of colocalizing particles at time t and I' is the initial number of colocalizing particles. Apparent lifetime values obtained with simulated particles (τ_1^*) provided an estimate of the duration of random colocalizations. Because the colocalizations observed in β_1-/β_2AR image sequences were expected to result either from random colocalization or from receptor interactions, data from β_1-/β_2AR image sequences were then fitted to the sum of two-exponential functions, using the equation

$$I = I_1' \cdot e^{-\frac{t}{\tau_1^*}} + I_2' \cdot e^{-\frac{t}{\tau_2^*}},$$

where I_1', I_2', and τ_2^* are unknowns. Once both τ_1^* and τ_2^* were estimated, the true lifetime of receptor interactions (τ_{int}) was calculated on the basis of the following equation (2):

$$\tau_{int} = \tau_2^* - \tau_1^*.$$

Correction for Random Colocalizations. We assumed that each image sequence contained particles of different size (i.e., containing a different number of receptors) and defined ρ_j as the density of particles with size j, where

$$j = 1, \ldots, n.$$

On the basis of our experimental data, we considered a maximum of $n = 7$ receptors per particle. We also defined the apparent density of particles with different size, i.e., those derived from the mixed Gaussian fitting analyses, as $\overline{\rho_j}$. The random colocalization of a particle with size i and another one with size j to give rise to a particle of apparent size $i + j$ can then be defined as

$$I + J \rightarrow \overline{IJ},$$

where we consider $i + j \leq n$.

Next, we performed laboratory experiments and data analyses to estimate the dependency of the density of apparent dimers on the density of monomeric control receptors (SNAP-CD86) as well as of simulated particles (Fig. S8*A*). We found that the density of apparent dimers ($\overline{\rho}_2$) was growing with the second power of monomer density (ρ_1) and fitted the data with the equation

$$\overline{\rho}_2 = a\rho_1^2,$$

allowing us to estimate $a = 0.4$ (based on SNAP-CD86 data).

Extending this to the general case of an interaction between a particle of size i and another one of size j and assuming that a is independent of i and j, the density of particles of apparent

size $i+j$ was then modeled by a bilinear colocalization function as follows:

$$\rho_{i+j} = a\rho_i\rho_j\ .$$

This function was used to determine the underlying particle densities (ρ_j) based on the apparent values ($\overline{\rho_j}$). Specifically, we assumed that $\overline{\rho_j}$ results from ρ_j plus all possible colocalizations of particles of different size resulting in the formation of particles of size j and minus all possible colocalizations of particles of size j with themselves or with particles of another size. In the case of colocalization of two particles of the same size, we introduced a multiplying factor of 2 to take into account the disappearance of two particles of equal size to form one of double size. Thus, we obtained the following nonlinear algebraic equations:

$$\begin{aligned}
&\rho_1 - a\rho_1(2\rho_1+\rho_2+\rho_3+\rho_4+\rho_5+\rho_6) - \overline{\rho}_1 = 0\\
&\rho_2 + a\rho_1^2 - a\rho_2(\rho_1+2\rho_2+\rho_3+\rho_4+\rho_5) - \overline{\rho}_2 = 0\\
&\rho_3 + a\rho_1\rho_2 - a\rho_3(\rho_1+\rho_2+2\rho_3+\rho_4) - \overline{\rho}_3 = 0\\
&\rho_4 + a\rho_1\rho_3 + a\rho_2^2 - a\rho_4(\rho_1+\rho_2+\rho_3) - \overline{\rho}_4 = 0\\
&\rho_5 + a\rho_1\rho_4 + a\rho_2\rho_3 - a\rho_5(\rho_1+\rho_2) - \overline{\rho}_5 = 0\\
&\rho_6 + a\rho_1\rho_5 + a\rho_2\rho_4 + a\rho_3^2 - a\rho_6(\rho_1) - \overline{\rho}_6 = 0\\
&\rho_7 + a\rho_1\rho_6 + a\rho_2\rho_5 + a\rho_3\rho_4 - \overline{\rho}_7 = 0.
\end{aligned} \qquad \textbf{[S1]}$$

In addition, we considered a linear combination of these equations to impose consistency of the formulation of the nonlinear system and conservation of the total number of receptors:

$$\begin{aligned}
\rho_1+2\rho_2+3\rho_3+4\rho_4+5\rho_5+6\rho_6+7\rho_7 = \overline{\rho}_1+2\overline{\rho}_2+3\overline{\rho}_3+4\overline{\rho}_4\\
+5\overline{\rho}_5+6\overline{\rho}_6+7\overline{\rho}_7.
\end{aligned} \qquad \textbf{[S2]}$$

For ease of discussion, we denote Eqs. **S1** and **S2** as

$$f_j(\rho) = 0,\ \ j = 1,\ldots,n+1,$$

where $\rho = (\rho_1,\rho_2,\rho_3,\rho_4,\rho_5,\rho_6,\rho_7)$. Further, we denote with $F(\rho) = (f_j(\rho))_{j=1}^{n+1}$ a column vector of functions. With this setting, the system containing Eqs. **S1** and **S2** can be formulated as $F(\rho) = 0$.

We remark that the problem $F(\rho) = 0$ may have no solutions because the measured data are affected by observation errors and the bilinear colocalization function represents an approximation to the microscopic colocalization function. For this reason, it is appropriate to solve $F(\rho) = 0$ with a least-squares method; i.e., we consider the following minimization problem. Find ρ^* such that

$$\| F(\rho^*) \| = \min_{\rho} \| F(\rho) \|,$$

where $\| \cdot \|$ denotes the Euclidean norm.

To solve this problem, a Gauss–Newton (GN) iterative scheme was used. Using Taylor expansion $F(\rho) = F(\rho^k) + F'(\rho^k)(\rho-\rho^k) + O(\rho-\rho^{k2}_2)$, we obtained a sequence of linear least-squares problems:

i) Find s^k with minimal Euclidean norm, such that

$$\| F'(\rho^k)s^k + F(\rho^k) \|_2 = \min_s \| F'(\rho^k)s + F(\rho^k) \|.$$

ii) Set $\rho^{k+1} = \rho^k + s^k$ and repeat until convergence.

If the linearized equations have full rank, i.e., $Rank(F'(\rho)) = n$, a minimal norm solution is obtained by the GN iteration. Otherwise, a Levenberg–Marquardt (LM) scheme is used to obtain the least-squares solution with minimal norm. In fact, the LM solver represents a regularized version of the GN scheme. It solves the following problem. Find s^k, such that

$$\begin{aligned}
\| F'(\rho^k)s^k + F(\rho^k) \|_2^2 + \mu^2 \| s^k \|_2^2 = \min_s (\| F'(\rho^k)s + F(\rho^k) \|_2^2\\
+\mu^2 \| s \|_2^2),
\end{aligned}$$

where $\mu > 0$ is a regularization parameter.

This solution process is implemented by the Matlab function lsqnonlin that we used in our code. Note that the additional Eq. **S2** improved the stability of the solution process.

1. Jaqaman K, et al. (2008) Robust single-particle tracking in live-cell time-lapse sequences. *Nat Methods* 5(8):695–702.
2. Kasai RS, et al. (2011) Full characterization of GPCR monomer-dimer dynamic equilibrium by single molecule imaging. *J Cell Biol* 192(3):463–480.
3. Suzuki K, Ritchie K, Kajikawa E, Fujiwara T, Kusumi A (2005) Rapid hop diffusion of a G-protein-coupled receptor in the plasma membrane as revealed by single-molecule techniques. *Biophys J* 88(5):3659–3680.
4. Krasel C, Bünemann M, Lorenz K, Lohse MJ (2005) β-arrestin binding to the β_2-adrenergic receptor requires both receptor phosphorylation and receptor activation. *J Biol Chem* 280(10):9528–9535.
5. Dorsch S, Klotz KN, Engelhardt S, Lohse MJ, Bünemann M (2009) Analysis of receptor oligomerization by FRAP microscopy. *Nat Methods* 6(3):225–230.
6. Maurel D, et al. (2008) Cell-surface protein-protein interaction analysis with time-resolved FRET and snap-tag technologies: Application to GPCR oligomerization. *Nat Methods* 5(6):561–567.
7. Hoffmann C, Leitz MR, Oberdorf-Maass S, Lohse MJ, Klotz KN (2004) Comparative pharmacology of human β-adrenergic receptor subtypes—Characterization of stably transfected receptors in CHO cells. *Naunyn Schmiedebergs Arch Pharmacol* 369(2): 151–159.
8. Brooker G, Harper JF, Terasaki WL, Moylan RD (1979) Radioimmunoassay of cyclic AMP and cyclic GMP. *Adv Cyclic Nucleotide Res* 10:1–33.
9. Mutch SA, et al. (2007) Deconvolving single-molecule intensity distributions for quantitative microscopy measurements. *Biophys J* 92(8):2926–2943.

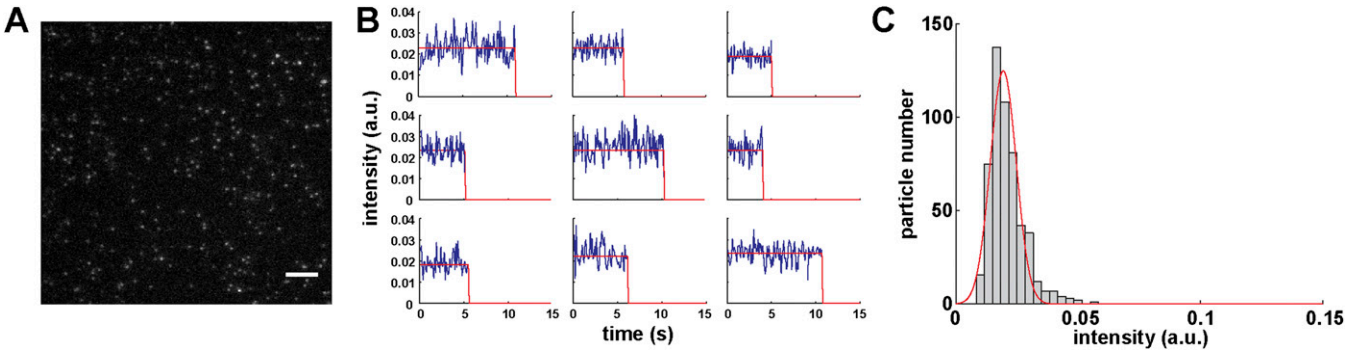

Fig. S1. Detection of single Alexa647-BG fluorophores by TIRF-M. (*A*) TIRF-M image of single Alexa647-BG molecules spotted on a clean glass coverslip. (Scale bar, 5 μm.) The position and intensity of each particle were automatically detected. (*B*) Representative intensity profiles (blue) of Alexa647-BG particles. Intensity profiles were fitted with a step-fitting algorithm (red). Single-step bleaching is observed, as expected for single molecules. (*C*) Intensity distribution of Alexa647-BG particles. Besides a largely predominant peak (red curve), an additional small peak of approximately double intensity was present, likely due to the random colocalization of two fluorophores.

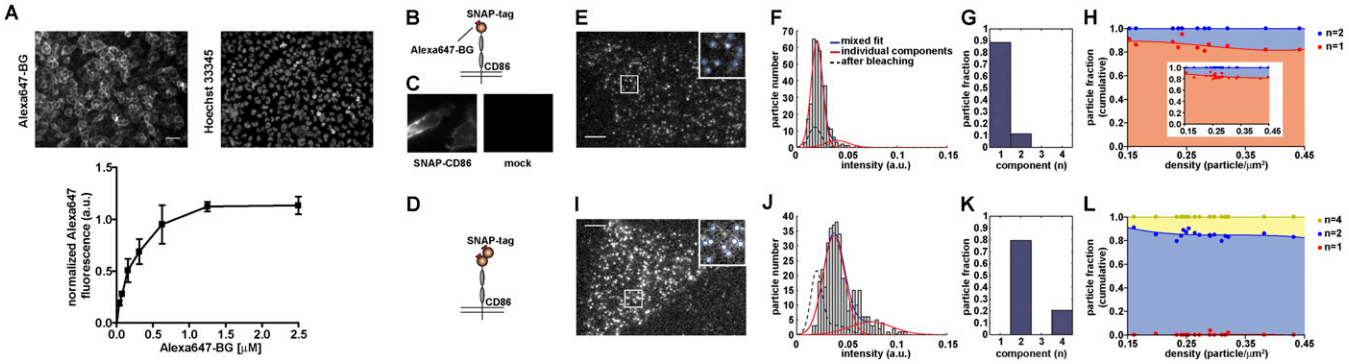

Fig. S2. Visualization of SNAP-tagged proteins on the surface of living cells (*A*) and validation of the single-molecule approach using control proteins with a single or with two labels (*B–L*). (*A*) Efficiency of SNAP-tag labeling. HEK293 cells stably expressing SNAP-β_1AR were stained with different concentrations of Alexa647-BG and the nuclear dye Hoechst 33345, used for normalization. Shown are data (means ± SEM) from a representative experiment performed in quadruplicate. (Scale bar, 100 μm.) (*B*) Schematic representation of a CD86 construct carrying one SNAP-tag at its N terminus (SNAP-CD86). (*C*) Epifluorescence images of cells transfected with SNAP-CD86 and control mock-transfected cells. (*D*) Schematic representation of a CD86 construct carrying two SNAP-tags at its N terminus (SNAP2×-CD86). Reported are the results obtained in cells transfected with either SNAP-CD86 (*E–H*) or SNAP2×-CD86 (*I–L*). (*E* and *I*) Representative images of single cells transfected with either construct, labeled and visualized by TIRF-M. (Scale bars, 5 μm.) *Insets* correspond to higher-magnification images of the areas in the white boxes; here detected particles are indicated by blue circles. Particle densities were 0.23 (*E*) and 0.31 (*I*) particle/μm^2. (*F* and *J*) Intensity distribution of Alexa647-labeled CD86 particles in *E* and *I*. Data were fitted with a mixed Gaussian model. (*G* and *K*) Abundance of individual components of the mixed Gaussian fits in *F* and *J*. n = 1, monomers. n = 2, dimers. n = 3, trimers. n = 4, tetramers. (*H* and *L*) Dependency of the distribution of particle components on particle density. Shown are the cumulative distributions of mono-, di-, and tetramers of Alexa647-labeled CD86, based on mixed Gaussian fitting analyses like those shown in *F* and *J*, as a function of particle density. Data were fitted using third-order polynomial functions. Each data point represents one cell [n = 1,965 particles from 11 different cells (*H*) and 3,127 particles from 17 different cells (*L*)]. (*H*, *Inset*) Same analysis in cells labeled with a low concentration (75 nM) of Alexa647-BG, resulting in ∼10% labeling efficiency.

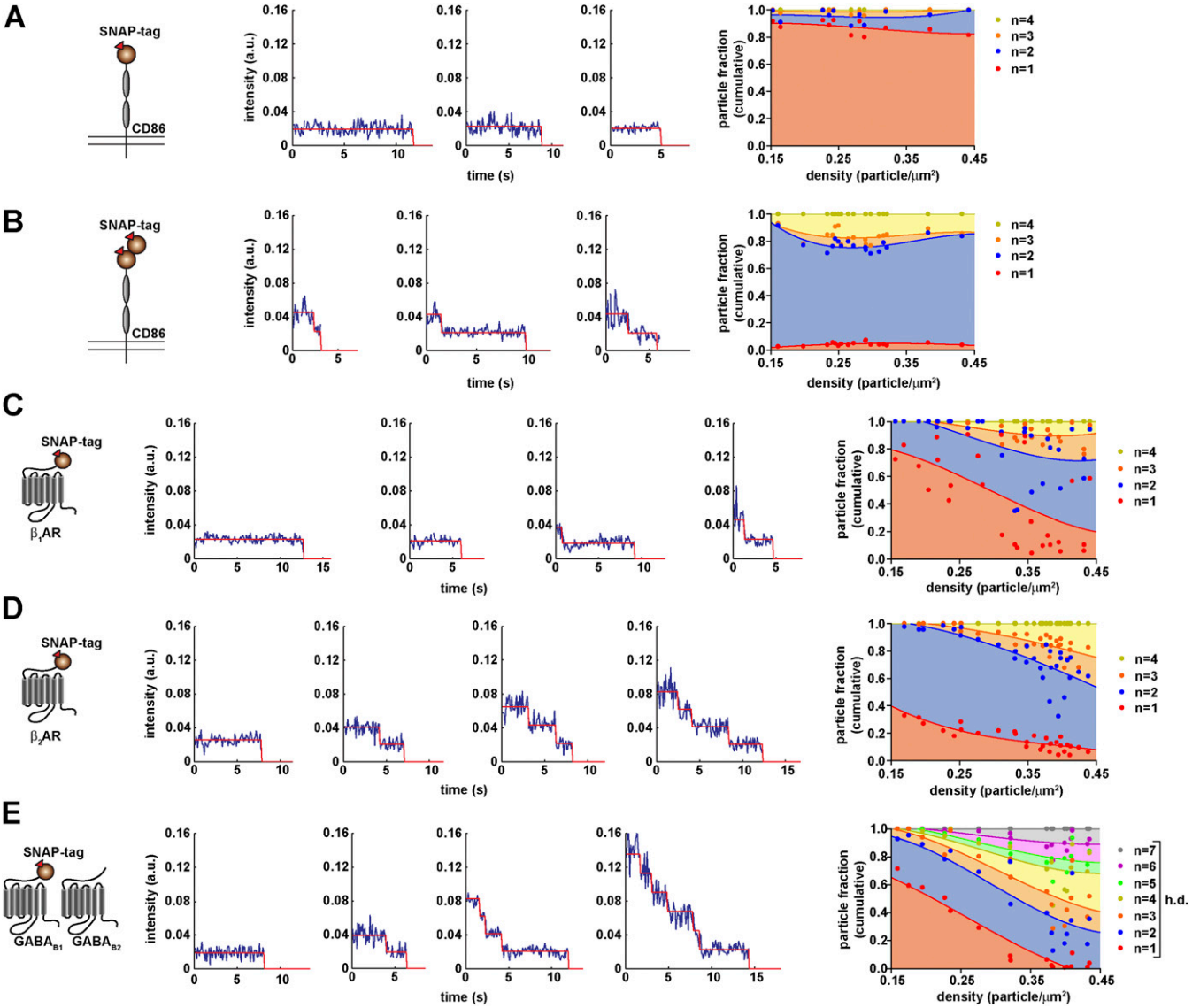

Fig. S3. Estimation of the size of receptor particles based on bleaching steps. (*A*–*E*) (*Left*) Representative intensity profiles (blue) and the results of the step-fitting algorithm (red) obtained with SNAP-CD86 (*A*), SNAP2×-CD86 (*B*), SNAP-β_1AR (*C*), SNAP-β_2AR (*D*), and SNAP-$GABA_{B1}$ plus wild-type $GABA_{B2}$ (*E*). (*Right*) Cumulative distributions of the abundance of receptor n-mers based on the results of the step-fitting analyses as a function of particle density. Data were fitted using third-order polynomial functions. Each data point represents one cell [n = 1,965 particles from 11 different cells (*A*), 3,127 particles from 17 different cells (*B*), 6,181 particles from 27 different cells (*C*), 7,419 particles from 30 different cells (*D*), and 4,472 particles from 17 different cells (*E*)].

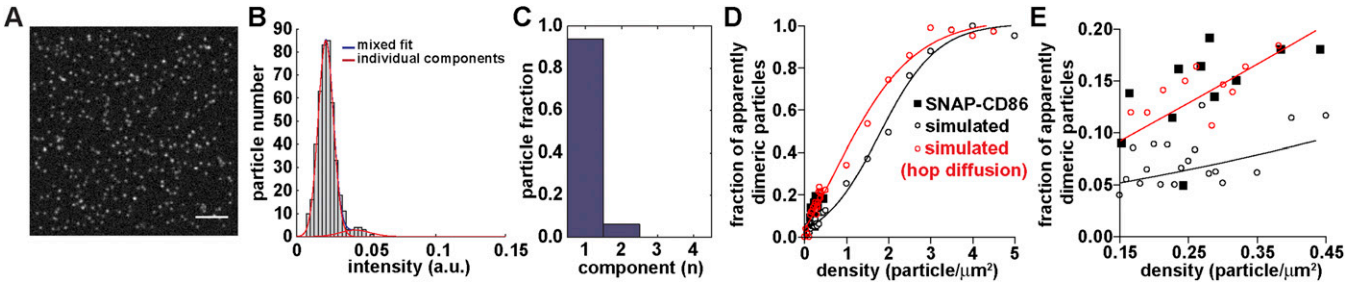

Fig. S4. Validation of the single-molecule approach, using simulated particles. Computer-generated image sequences containing particles moving with Brownian motion and characteristics (diffusion coefficients, intensity distribution, bleaching rate) similar to those of Alexa647-labeled SNAP-CD86 particles were analyzed as described in Fig. S2. (*A*) First image of a typical simulated movie. Particle density = 0.35 particle/μm^2. (Scale bar, 5 μm.) (*B*) Intensity distribution of simulated particles in *A*. Data were fitted with a mixed Gaussian model. (*C*) Abundance of individual components of the mixed Gaussian fitting in *B*. $n = 1$, monomers. $n = 2$, dimers. $n = 3$, trimers. $n = 4$, tetramers. (*D*) Dependency of the fraction of particles detected as apparently dimeric on particle density. The results obtained with SNAP-CD86 and simulated particles are compared. Red data refer to simulations of particles with "hop" diffusion [$n = 12{,}445 + 8{,}615$ simulated particles from 39 + 27 simulations and 1,965 SNAP-CD86 particles from 11 different cells]. (*E*) Detailed view of the data in *D* over the particle densities used in the present study.

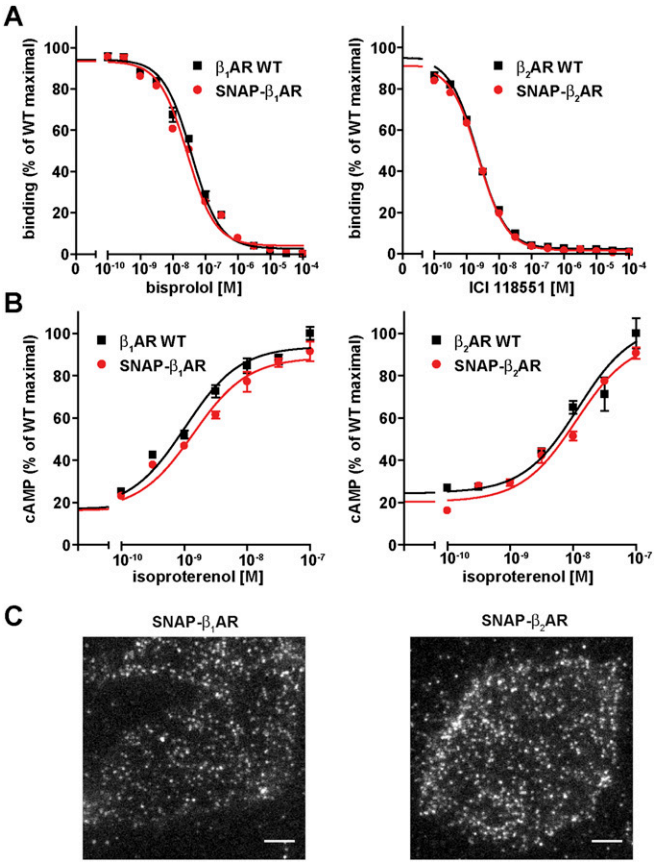

Fig. S5. Functional characterization and single-molecule visualization of SNAP-tagged β_1- and β_2AR constructs. (*A*) Radioligand binding. CHO cells were transfected with SNAP-tagged β_1AR, β_2AR, or wild-type receptors. Membranes were incubated with 50 pM [^{125}I]iodocyanopindolol and the indicated concentrations of bisprolol or ICI-118551. Data are means ± SEM of four replicates from two independent experiments. (*B*) cAMP assay. CHO cells were transfected with SNAP-tagged β_1AR, β_2AR, or wild-type receptors and stimulated with the indicated concentrations of isoproterenol. Data are means ± SEM of three independent experiments. (*C*) Visualization of individual receptors on the surface of living cells. Shown are representative images of cells transfected with SNAP-β_1AR or SNAP-β_2AR, labeled with Alexa647-BG and visualized by TIRF-M. (Scale bars, 5 μm.)

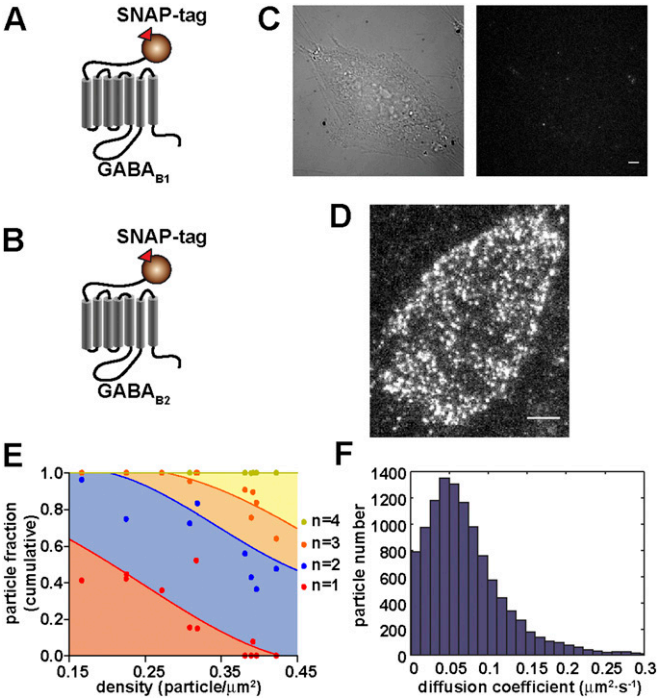

Fig. S6. Analysis of individually expressed SNAP-GABA$_{B1}$ and SNAP-GABA$_{B2}$ subunits. (*A* and *B*) Cells were transfected with either construct alone, labeled with Alexa647-BG, and visualized by TIRF-M. (*C*) Representative image (*Left*, brightfield; *Right*, TIRF) of a cell transfected with SNAP-GABA$_{B1}$. No cell-surface staining is present. (*D*) Representative image of a cell transfected with SNAP-GABA$_{B2}$. Single receptor particles are visible. Particle density = 0.42 particle/μm^2. (*E*) Dependency of the distribution of particle components in cells transfected with SNAP-GABA$_{B2}$ on particle density. Particle composition is based on mixed Gaussian fitting analyses and is represented as in Fig. S2 *H* and *L* (n = 3,580 particles from 12 different cells). (*F*) Distribution of diffusion coefficients of SNAP-GABA$_{B2}$ particles. (Scale bars, 5 μm.)

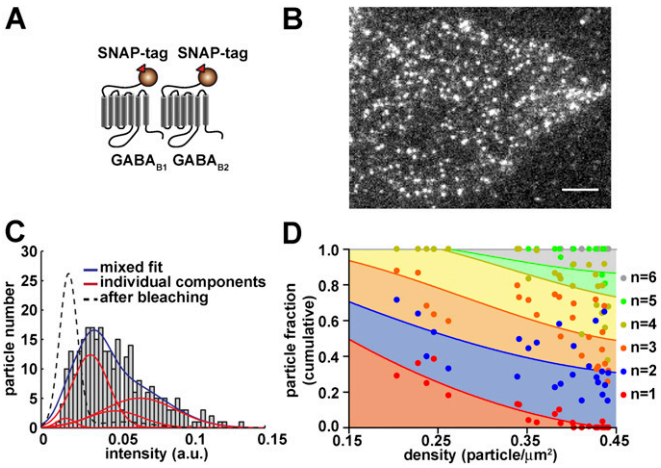

Fig. S7. Single-molecule analysis of coexpressed SNAP-GABA$_{B1}$ and SNAP-GABA$_{B2}$. (*A*) Schematic representation of the used SNAP-tagged constructs. (*B*) Representative image of cells transfected with both constructs, labeled with Alexa647-BG, and visualized by TIRF-M. (Scale bar, 5 μm.) Particle density was 0.36 particle/μm^2. (*C*) Intensity distribution of Alexa647-labeled particles in *B*. Data were fitted with a mixed Gaussian model. (*D*) Dependency of the distribution of particle components on particle density. Particle composition is based on mixed Gaussian fitting analyses as in *C* and is represented as in Fig. S2 *H* and *L* (n = 7,399 particles from 25 different cells).

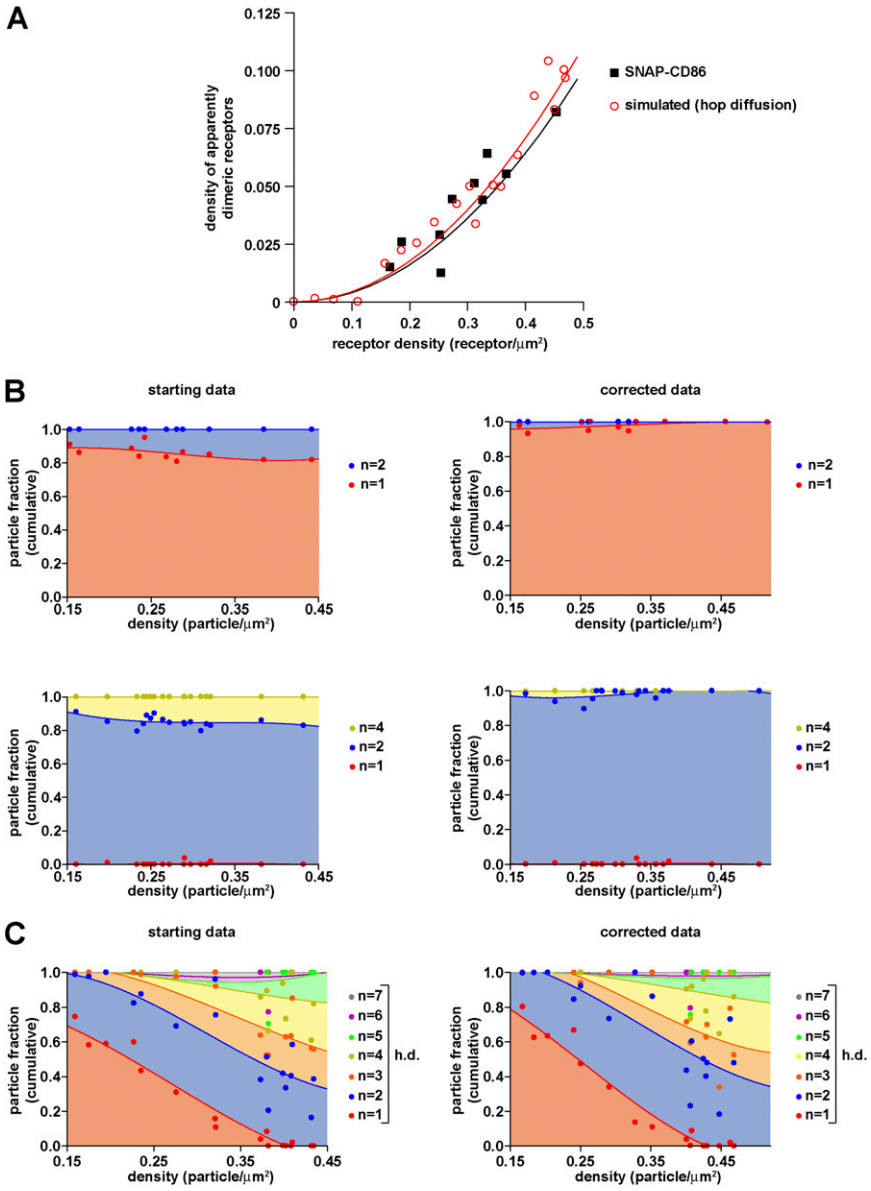

Fig. S8. Correction of particle distributions for random colocalizations. (*A*) Dependency of the density of apparent dimeric receptors on the density of monomeric control receptors (SNAP-CD86) or simulated particles. Raw data are the same as those used in Fig. S4. (*B*) Correction of SNAP-CD86 and SNAP2×-CD86 particle distributions for the presence of random colocalizations. *Left*, starting data; *Right*, data after correction. (*C*) Same correction applied to the $GABA_B$ data shown in Fig. 4*D*.

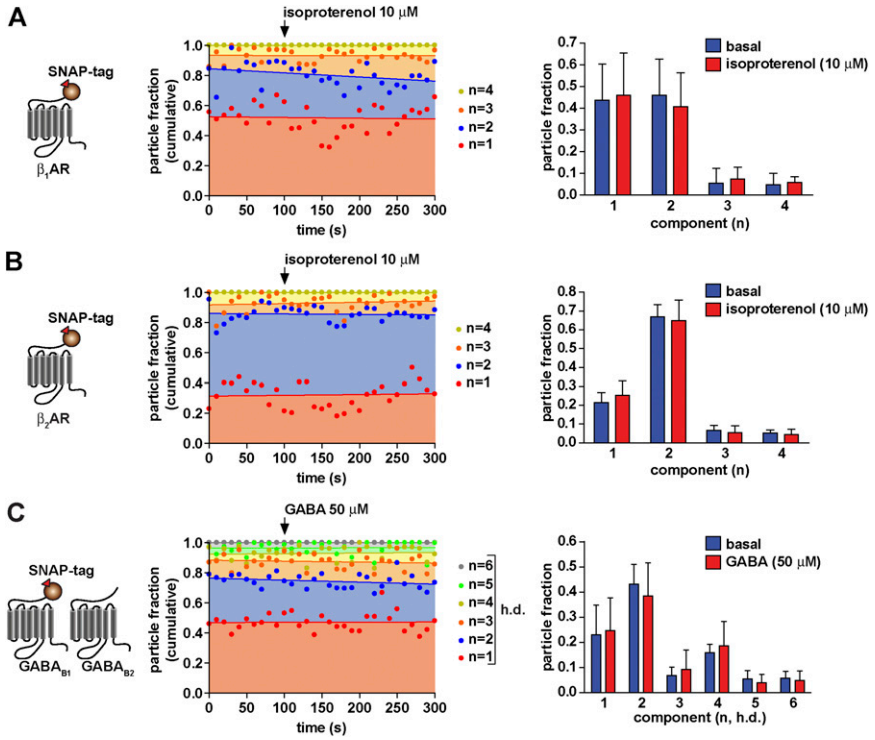

Fig. S9. Effect of agonists on receptor di-/oligomerization. (*A*–*C*) Cells were transfected with SNAP-β_1AR (*A*), SNAP-β_2AR (*B*), or SNAP-$GABA_{B1}$ plus wild-type $GABA_{B2}$ (*C*) constructs; labeled with Alexa647-BG; and visualized by TIRF-M. To limit particle photobleaching, images were acquired every 10 s for 300 s, which resulted in less than 15% photobleaching at the end of the acquisition. The particles in the resulting image sequences were detected as in Fig. S1, without tracking. For each time point, particle intensities in three consecutive frames were used to perform a mixed Gaussian fitting analysis. (*Left*) Results of three representative experiments. The graphs report the composition of receptor particles, derived from the mixed Gaussian fitting analyses, as a function of time. For β_1AR and β_2AR: $n = 1$, monomers; $n = 2$, dimers; $n = 3$, trimers; $n = 4$, tetramers. For $GABA_B$: $n = 1$, one heterodimer; $n = 2$, two heterodimers, $n = 3$, three heterodimers, etc. (*Right*) Summary of the results obtained from six experiments per each condition. The mean (±SD) abundance of each component before and 300 s after agonist stimulation is reported. Differences between stimulated and basal are not statistically significant by paired two-way ANOVA.

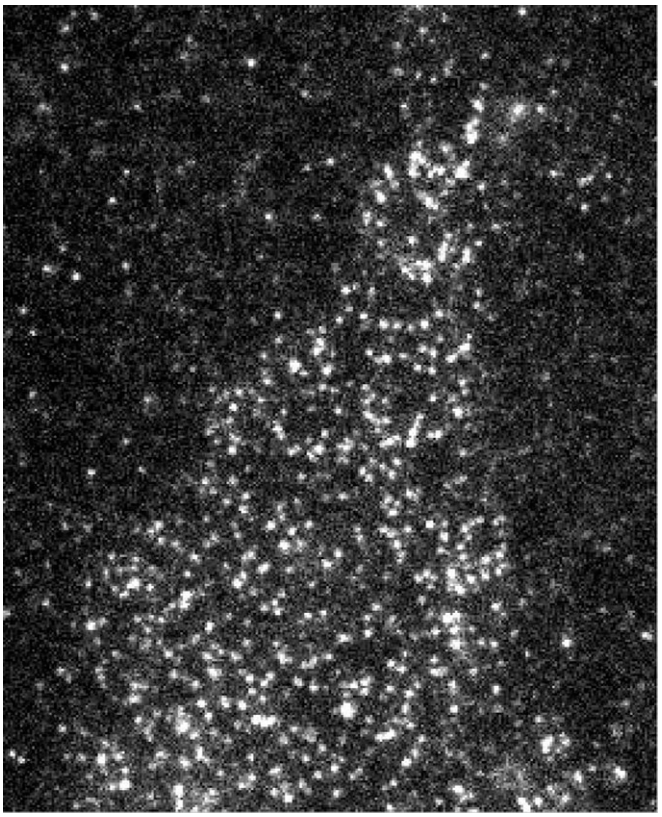

Movie S1. TIRF-M image sequence of Alexa647-labeled SNAP-CD86 receptors on the surface of a living cell.

Movie S1

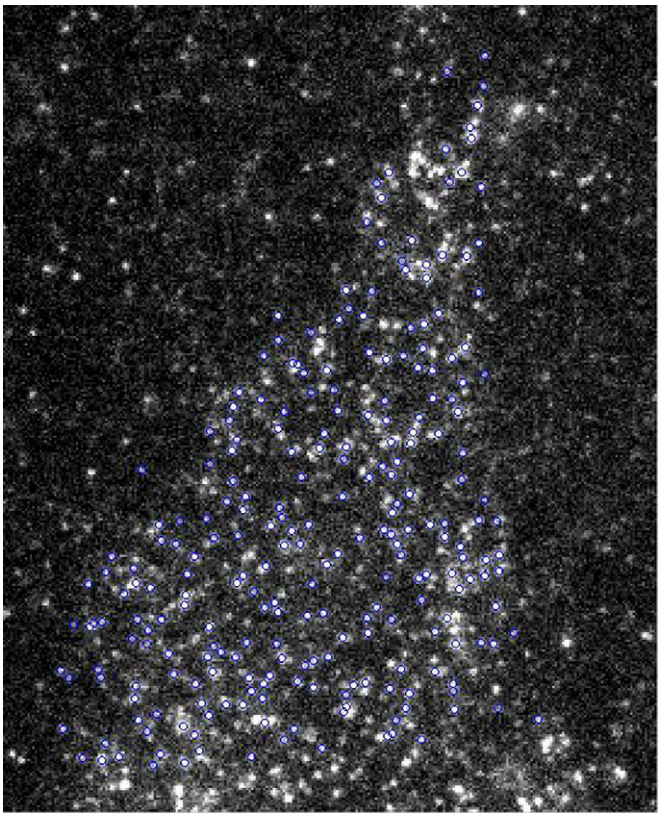

Movie S2. Result of particle tracking analysis of the image sequence in Movie S1.

Movie S2

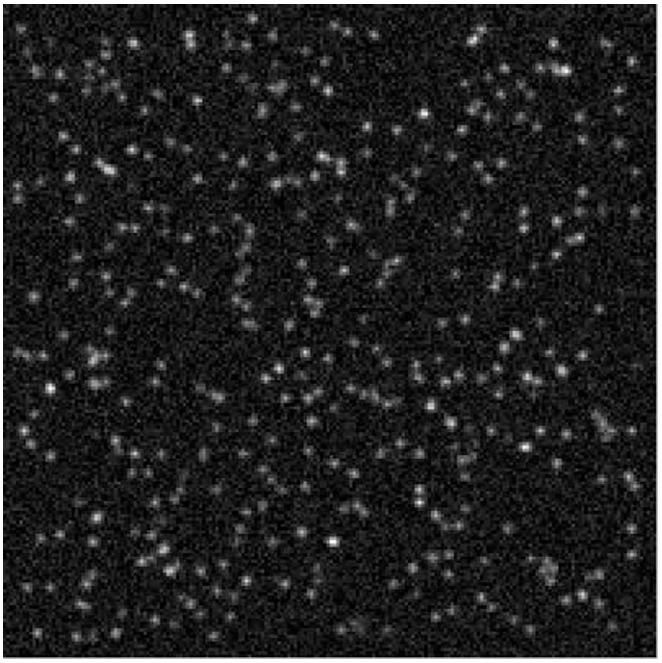

Movie S3. Computer-generated image sequence containing simulated particles with Brownian motion and characteristics (diffusion coefficients, intensity distribution, bleaching rate) similar to those of Alexa647-labeled SNAP-CD86 particles.

Movie S3